AGU ADVANCING EARTH AND SPACE SCIENCES

Geophysical Research Letters

RESEARCH LETTER
10.1029/2024GL112870

Ku- and Ka-Band Polarimetric Radar Waveforms and Snow Depth Estimation Over Multi-Year Antarctic Sea Ice in the Weddell Sea

Rosemary Willatt[1,2], Robbie Mallett[1,3,4], Julienne Stroeve[1,4,5], Jeremy Wilkinson[6], Vishnu Nandan[7,8], and Thomas Newman[1]

[1]Department of Earth Sciences, UCL, London, UK, [2]Centre for Polar Observation and Modelling, Geography and Environmental Sciences, Northumbria University, Newcastle upon Tyne, UK, [3]Earth Observation Group, Department of Physics and Technology, UiT the Arctic University of Norway, Tromsø, Norway, [4]Centre for Earth Observation Science, Clayton H. Riddell Faculty of Environment, Earth and Resources, University of Manitoba, Winnipeg, MB, Canada, [5]National Snow and Ice Data Center, Boulder, CO, USA, [6]British Antarctic Survey, Cambridge, UK, [7]Department of Electronics and Communication Engineering, Amrita Vishwa Vidyapeetham, Bengalaru, India, [8]Department of Geography, University of Calgary, Calgary, AB, Canada

Key Points:

- Radar measurements and coincident geophysical data were collected over five multi-year sea ice floes in the Weddell Sea
- A remnant layer of metamorphosed snow which had survived the summer melt lay beneath snow deposited during the current cold season
- Co-polarized scattering occurred close to the air/snow interface and polarimetric techniques showed promise for snow depth retrieval

Supporting Information:

Supporting Information may be found in the online version of this article.

Correspondence to:

R. Willatt,
r.willatt@ucl.ac.uk

Citation:

Willatt, R., Mallett, R., Stroeve, J., Wilkinson, J., Nandan, V., & Newman, T. (2025). Ku- and Ka-band polarimetric radar waveforms and snow depth estimation over multi-year Antarctic sea ice in the Weddell Sea. *Geophysical Research Letters*, *52*, e2024GL112870. https://doi.org/10.1029/2024GL112870

Received 24 JAN 2025
Accepted 1 JUN 2025

Author Contributions:

Conceptualization: Robbie Mallett
Data curation: Robbie Mallett
Formal analysis: Rosemary Willatt
Funding acquisition: Julienne Stroeve, Jeremy Wilkinson
Investigation: Rosemary Willatt, Robbie Mallett, Jeremy Wilkinson
Methodology: Rosemary Willatt, Robbie Mallett
Project administration: Julienne Stroeve, Jeremy Wilkinson
Software: Rosemary Willatt, Vishnu Nandan
Supervision: Julienne Stroeve
Visualization: Rosemary Willatt

Abstract Antarctic sea ice has seen recent rapid declines in extent, but it remains unclear whether this is accompanied by thinning. Due to the relative abundance and complexity of overlying snow on sea ice, radar altimetry methods routinely deployed for sea ice thickness estimation in the Arctic are difficult to apply in Antarctica. We present nadir-looking radar waveforms from the first deployment of the KuKa surface-based radar on Antarctic sea ice, specifically multi-year sea ice in the Weddell Sea marginal ice zone with a thick snow cover. Coincident snow pits revealed thick layers of snow which were exposed to the summer melt season and superimposed ice. Our instrument detects only very small amount of co-polarized radar backscatter from the sea ice surface, suggesting that conventional satellite altimeters may not always range to this interface. However, polarimetric snow depth determination performs well, with r^2 of 0.76 between measured and KuKa-estimated snow depths.

Plain Language Summary The area of sea ice surrounding Antarctica has recently been declining, but it is uncertain whether it is also getting thinner. That uncertainty is because we cannot effectively monitor sea ice thickness with satellite-mounted radar instruments when the snow on top of the sea ice blocks the radar waves. During a research ship cruise in the Weddell Sea, we scanned a set of complex snow packs using a high-resolution, surface-based radar. Our data suggest that the methods conventionally deployed in the Arctic would not work well at our field sites. However, a recently proposed, new method of snow depth determination based on a previous Arctic deployment of the same instrument was effective.

1. Introduction

Following small positive trends in Southern Ocean sea ice extent until 2014, recent reductions in sea ice minimum extent around Antarctica have resulted in the trends turning negative. All-time minimum austral summer extents were reached in 2022 (Turner et al., 2022) (with the Weddell contributing 26%) and 2023 (Purich & Doddridge, 2023), with a historically low rate of areal growth in winter of 2023 (Gilbert & Holmes, 2024).

While changes in Antarctic sea ice area have been observed using microwave radiometers since the late 1970s, estimating Antarctic sea ice thickness remains challenging. Part of the challenge lies in conventional assumptions applied to the location of the dominant scattering surface of radar altimeters. Sea ice thickness retrieval algorithms using Ku-band satellite radar altimeters, such as ESA's CryoSat-2, are routinely used in the Arctic, under the assumption that the sea ice surface is the dominant scattering surface (e.g., Laxon et al., 2003). Studies have challenged this assumption (Nab et al., 2023; Ricker et al., 2015; Willatt et al., 2011, 2023), and specific features of snow cover on Antarctic sea ice suggest that assumptions used in the Arctic are less likely to be valid here.

Giles et al. (2008) studied the feasibility of sea ice thickness estimates using satellite radar altimetry in Antarctica. Comparisons with Antarctic Sea Ice Processes and Climate (ASPEcT) data (Worby et al., 2008), which contains pan-Antarctic ship-based observations of snow and sea ice thickness, led Giles et al. (2008) to believe that the key assumption used in the Arctic, that the snow/sea ice interface is the dominant scattering surface, was likely not the

Writing – original draft: Rosemary Willatt, Robbie Mallett
Writing – review & editing: Rosemary Willatt, Julienne Stroeve, Jeremy Wilkinson, Vishnu Nandan, Thomas Newman

case and that scattering was occurring higher in the snow pack. This indicated that the method of Laxon et al. (2003) could not be directly applied for use in Antarctica. These results were supported by (Willatt et al., 2010) using surface-based radar and snow pit data.

These previous studies have important implications for snow depth retrievals using dual frequency altimeters. Kacimi and Kwok (2020) compared ICESat-2 and CryoSat-2 elevations with ASPEcT data, and found that retrieved snow thicknesses were too small and ice thicknesses were too large. Garnier et al. (2022) used Ku- and Ka-band altimetry combined with Advanced Microwave Scanning Radiometer data. In the Weddell sea, mean sea ice draft was overestimated by ~11 cm between May and September, and underestimated by ~40 cm in October, compared to Upward Looking Sonar data. There are particular challenges to remote sensing of sea ice in the Weddell Sea, where the sea ice is covered by snow year-round (Arndt et al., 2024), resulting in a snowpack that has undergone repeated freeze/thaw events. This can result in meltwater percolating either into inclusions in the ice (Ackley et al., 2008), or accumulating near the base and then freezing in winter to form superimposed ice (e.g., Haas et al. (2001), Arndt et al. (2021)). A recent advance in snow depth estimation over Antarctic sea ice by (Lawrence et al., 2024) used accumulated snowfall from the ERA5 atmospheric reanalysis. They assumed that a fixed fraction of 55% of snowfall was converted to snow-ice, which could introduce a significant error for positive freeboard scenarios such as those in this paper. Our investigation was designed to test the underlying assumptions and possibility of Antarctic snow depth retrievals with radar altimetry. We present Ku- and Ka-band radar waveforms from snow-covered multi year sea ice in the marginal ice zone of the Weddell Sea during Austral autumn of 2022.

2. Methods

2.1. Floe Selection

The Ka/Ku band fully-polarimetric radar (KuKa) (Stroeve et al., 2020) was deployed on five sea ice floes as part of a ship-based transect of the Weddell Sea's marginal ice zone in April 2022 (Figures 1a and 1b). Floes at least 50 cm thick were selected for safety reasons, leading to sampling of multi year floes, rather than thinner first year ice that was also present. The work was conducted shortly after the seasonal freeze-up, with surface air temperatures consistently below zero. Tracing of the floe trajectories can be found in the Text S1 in Supporting Information S1.

2.2. Snow Sampling and Radar Measurement Protocols

The low ice concentration and small floe sizes dictated collecting KuKa and snow depth data along a transect (e.g., Willatt et al. (2023)) was not feasible. Instead, a series of snow pit studies were carried out, similar to the approach of Willatt et al. (2010).

At 17 sites across the five multi-year ice floes, nadir-looking Ku- and Ka-band radar waveforms were first collected, followed by destructive sampling of snow geophysical properties. Care was taken to ensure that the antenna-horns of both radar instruments were sequentially and exactly aligned above the patch of snow, before a snow-pit was dug in the center of the patch. Where possible, geophysical observations taken at snow pits included vertical profiles of snow density, salinity and temperature, and grain characteristics such as size and shape. A synopsis of stratigraphy was taken, with measurements made layer-wise rather than at regular intervals. It was frequently not possible to dig to the snow-ice interface due to dense overlying snow (discussed in the Section 3 below). In these cases, we estimated the snow depth by using an ice corer–this was possible at 14 snow pits; at three snow pits we were unable to distinguish the remnant snow/sea ice interface so these are not included in our analysis.

2.3. Radar Processing and Waveform Adjustment

Radar data were processed using KuKaPy software (Mead et al., 2023) which processes the data from its raw form and outputs it as a series of netCDF files containing the waveforms, times, range bins etc. Many radar waveforms were generated in both frequencies for each site, and are averaged in the results that follow. Random noise in KuKa waveforms is low (Figure S3 of Willatt et al. (2023)) and the waveforms show little variation when the instrument is static (see Table S2 in Supporting Information S1 and Waveform Averaging for further information). Ka-band waveforms were shifted in range so that the air/snow interface was aligned with the Ku-band

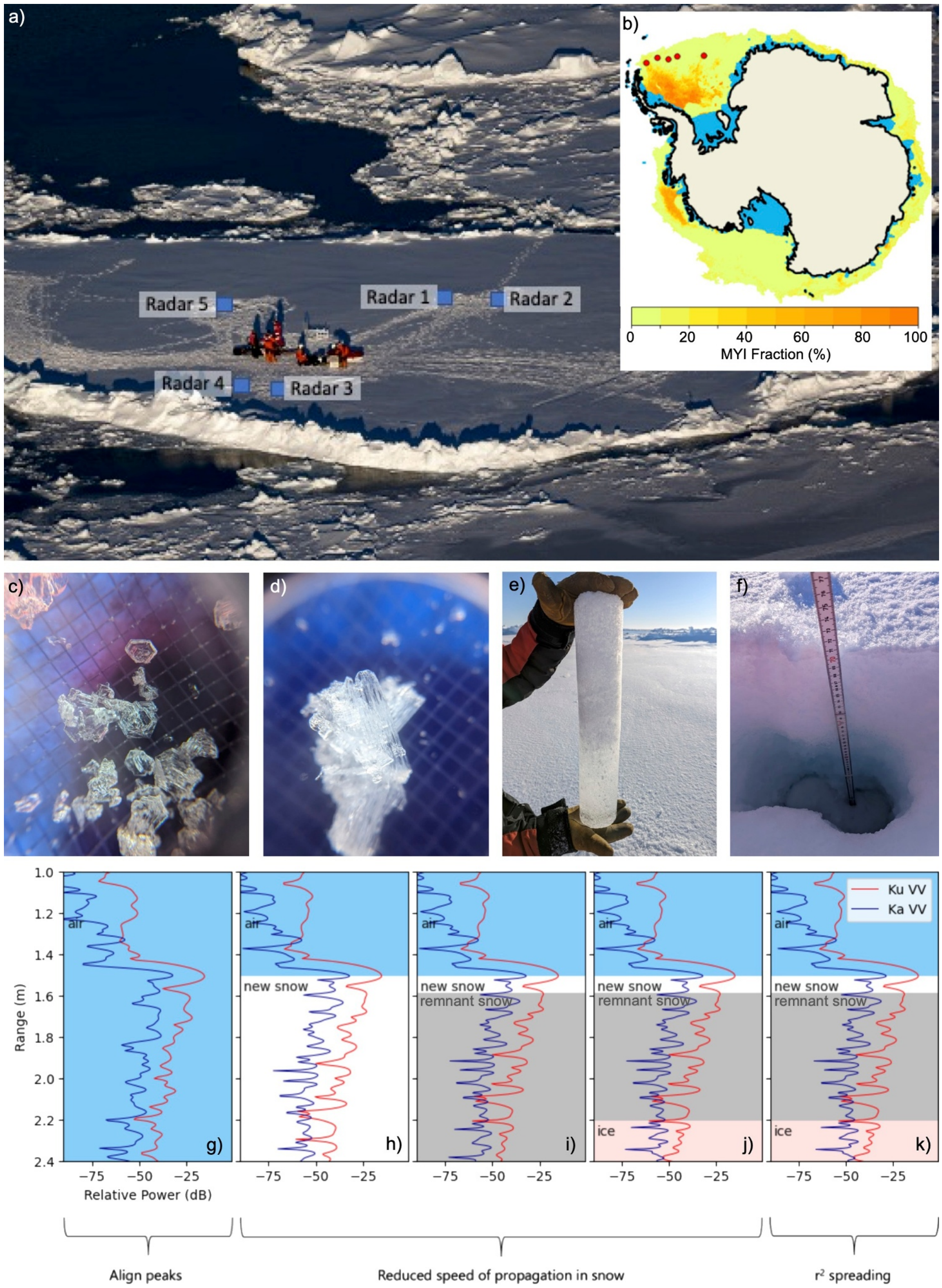

Figure 1. (a) Floe 5 (April 22nd) with five locations where data were collected (photograph by Jeremy Wilkinson). (b) Floe locations (red circles) superimposed on MYI fraction (Melsheimer et al. (2023) data) on April 22nd with blue indicating NSIDC ice shelf mask (Meier & Scott Stewart, 2023). (c) Photograph through a magnifying lens of highly faceted remnant snow at D1 SP1, with a 2 mm grid in the background. The highly sintered grains had been disaggregated with persistent tapping. (d) As panel (c), for a cluster of snow grains at D4 SP1. A high degree of grain anisotropy is present with long, linear metamorphic features sometimes in excess of 8 mm long. Grains were sufficiently sintered that they could not be fully disaggregated. (e) Snow core from Floe 5. Hard, remnant snow near the top of the core transitions to superimposed ice at the bottom. The snow depth could not be rigorously determined as the interface between the sea ice and superimposed ice could not be determined. (f) Snow pit at D3 SP2. Sequential adjustments to D3 SP2 waveforms are shown for peak alignment (green box) between Ku- and Ka-band data (g), reduced velocity of radiation as it propagates through snow with the addition of new snow (h), remnant snow (i) and ice (j), and finally accounting for beam spreading by multiplying the returned power in each range bin by r^2 (k).

waveforms using the VV co-polarized data; the resulting magnitude of this shift was between 1.0 and 5.3 cm. This was necessary because KuKa had to be shifted to align Ku- and Ka-band antennas over the same sampling area, due to the ~80 cm separation between Ku- and Ka-band horns.

We compensated for the reduced speed of microwave propagation in snow, compared to air based on layer-wise densities, similar to Willatt et al. (2010). The sea ice was not sampled, so a value of three for the dielectric constant was assumed based on typical values for sea ice from Figures 4–14 in Ulaby et al. (2014). Adjustments to the range were made layer by layer vertically downwards, starting from the new snow layer, similar to an "optical path length" calculation. For an interface closest to range bin number i ($range_i$), all range bins below this ($range_{i+n}$, where $n \geq 1$) were adjusted as follows:

$$range'_{i+n} = range_i + c' \left(range_{i+n} - range_i\right)$$

Where c' is the relative speed of radiation in the snow compared to air, and $range'_{i+n}$ is the new range at bin $i + n$, following adjustment. The compression of the waveform in range as the dielectric constant increases from air to new snow, remnant snow and then ice. We then accounted for the spreading of the radiation, by multiplying the power in each range bin by the square of the range $\left(r^2\right)$. This is analogous to the r^2 dependence in the traditional equation for the normalized radar cross-section of a distributed target (Ulaby et al., 2014). We note however that our results are qualitatively insensitive to this adjustment (Text S1 Additional Results and Figures S5 and S6 in Supporting Information S1). See Figures 1g–1k for illustration of the adjustments.

2.4. Waveform Examination and Snow Depth Estimation Techniques

This study benefits from coincident snow pits and KuKa radar data, so we were able to overlay the two data sets and to make a visual inspection to determine where in the snow pack scattering is occurring. KuKa range resolution in air is 2.5 cm for the Ku-band, and 1.5 cm in the Ka-band, when using full bandwidth data (before Hann windowing). Satellite-based CryoSat-2 SIRAL (Wingham et al., 2006) and SRAL AltiKa (Vincent et al., 2006) altimeters operate at the same frequencies but with smaller bandwidths, resulting in 46 and 30 cm range resolution, respectively. The finer KuKa range resolution allows us to examine where in the snow pack scattering occurs, which cannot be resolved using the satellite sensors. We then used polarization techniques to estimate snow depth using polarimetric KuKa data and compared these to measured snow depths. For each waveform we calculated the range of the highest amplitude peak and the waveform centroid, which can be thought of as its center of gravity. Then we difference the ranges between the co-pol and cross-polarized peaks, and co-pol and cross-polarized centroids for our snow depth estimations. We calculate centroids using a standard power-weighted range, over 1 to 3 m as per Willatt et al. (2023) (their SI Equation 1). We display waveforms in dB for clear visualization, but centroids were calculated in linear power.

3. Results

The state and depth of the snow overlying the sea ice indicated that the sampled floes had survived the summer melt season, as opposed to having formed since freeze-up (in line with the floe tracing in Text S1 in Supporting Information S1). A layer of dense, hard, heavily metamorphosed *remnant snow* that had survived the summer melt period lay beneath a layer of softer, lower density *cold-season snow* that appeared to not have been exposed to above-zero temperatures in a way that initiated melt processes. When examined, the remnant snow layers often exhibited strongly faceted grains which were often several millimeters in length (Figures 1c and 1d). The base of the remnant snow layers sometimes transitioned into superimposed ice (Figure 1e). The degree to which this vertical snowpack structure represents sea ice in the Weddell Sea and Antarctica more broadly is discussed in Section 4; snow layering on the surrounding first year ice may be different but could not be sampled.

During the study the snowpack was cold and dry, confirmed with layer-wise snow pit temperature measurements which reached a maximum of $-3°$ Centigrade (SI Temperature Profiles). Analysis of snow salinity indicated that the snow was consistently fresh, so could not have been subjected to flooding due to negative ice freeboard. Flooding would reduce the likelihood of the snow/ice interface being the dominant scattering surface (Willatt et al., 2010).

Figure 2 shows examples from four snow pits selected to demonstrate diverse snow and waveform properties, with adjustments made as per Section 2.3. A Waveform Atlas containing waveforms from all snow pits can be found in the SI.

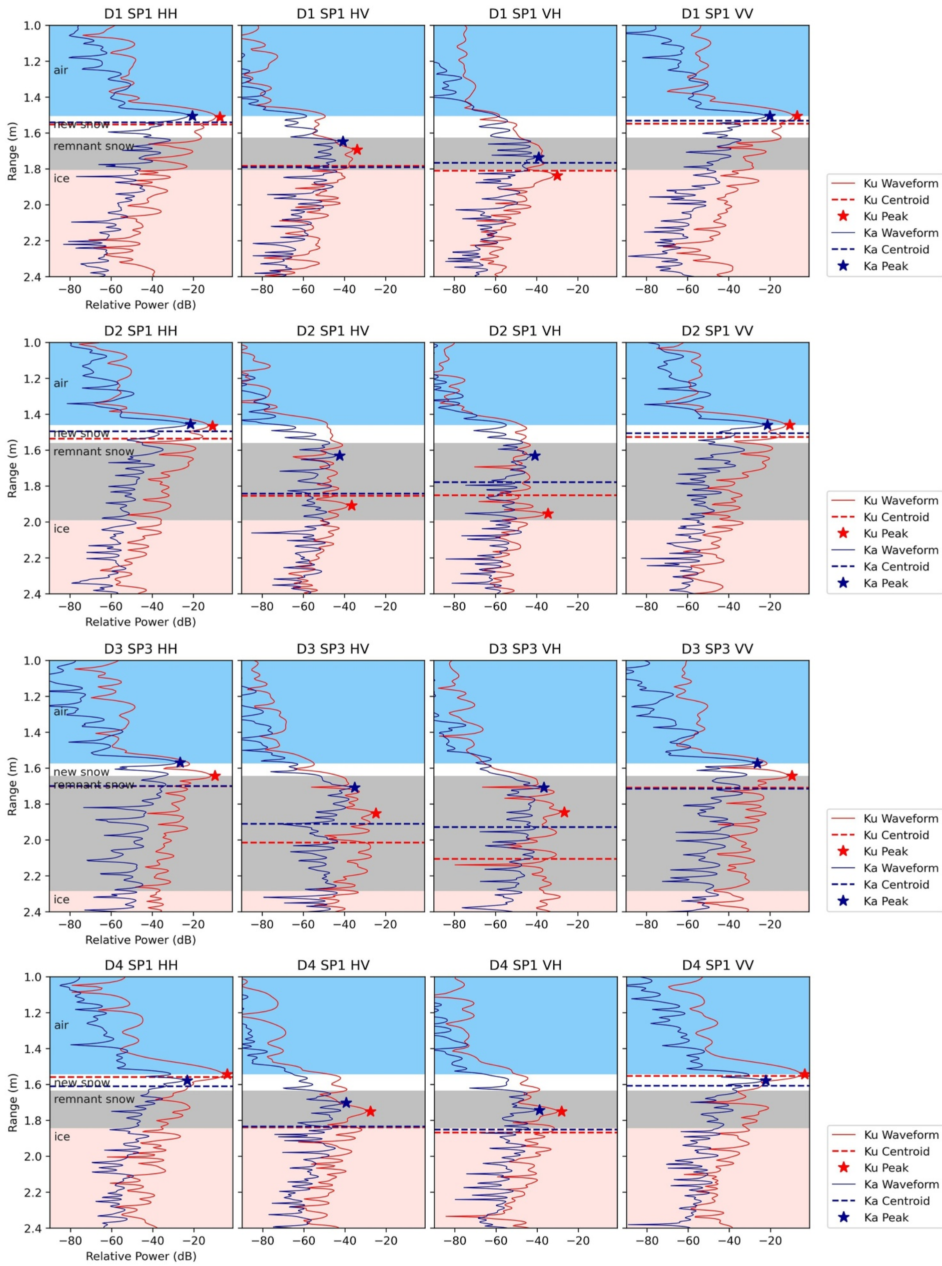

Figure 2. Four examples of sets of waveforms collected at snow pits: D1 SP1, D2 SP1, D3 DP3 and D4 SP1, with waveform peaks aligned and adjusted for reduced velocity through snow and r^2 spreading. Four panels (horizontally) per snow pit show the different polarizations for both Ku- and Ka-band data. Waveform centroids (dashed lines) and highest amplitude peaks (stars) are overlaid.

Total measured snow depths ranged from 20.5 to 71 cm with a mean of 46 cm, remnant snow depths from 0 to 64 cm with a mean of 38 cm, and new snow depths from 1 to 20.5 cm with a mean of 11 cm. New snow densities were between 208 and 333 gcm^{-3} with a mean of 275 gcm^{-3}. Remnant snow densities could only be measured in four snow pits, and ranged from 402 to 504 gcm^{-3} with a mean of 442 gcm^{-3}. The depths are shown for all pits in Figure 3a, relationships between depths in Figures 3b–3d and all snow depths and densities are listed Table S1 in Supporting Information S1).

We focus on HH waveforms to represent co-polarization, and VH waveforms to represent cross-polarization, due to AltiKa and CryoSat-2 using HH polarization configurations (Vincent et al., 2006; Wingham et al., 2006). VH

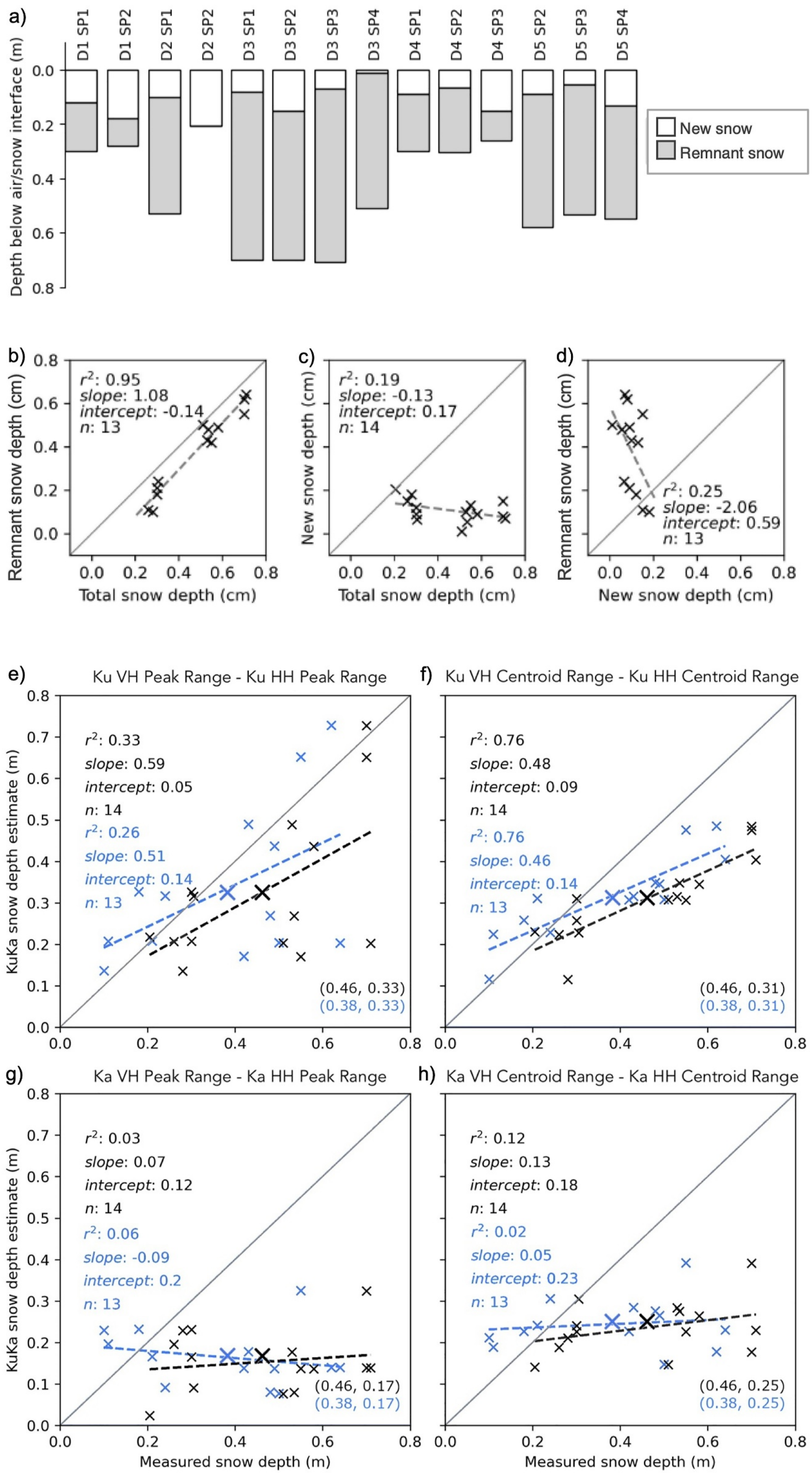

Figure 3. (a) Visualization of new and remnant snow depths. (b–d) Relationships between measured depths. (e–h) KuKa-estimated depths (y-axes) against ruler-measured total depths (x-axes) with number of points (n), and linear regression (dashed line) r^2, slope and intercept values. Black and blue indicate total and remnant measured depths, respectively. Coordinates of mean values (large crosses) are given at the bottom right.

Table 1
Mean Depths of the Highest Amplitude Peak and Centroid, as Depths Below the Air/Snow Interface and as a Percentage of Total Snow Depth, With Standard Deviations (STDs) Indicated

Band	Pol	Peak (m)	STD (m)	Centroid (m)	STD (m)	Peak (%)	STD (%)	Centroid (%)	STD (%)
Ku	HH	0.01	0.02	0.08	0.04	3	6	20	15
Ku	VV	0.01	0.02	0.07	0.03	1	3	18	12
Ku	VH	0.34	0.17	0.39	0.11	77	27	91	29
Ku	HV	0.32	0.18	0.37	0.1	75	39	88	32
Ka	HH	0.02	0.06	0.08	0.06	10	28	21	26
Ka	VV	0.02	0.06	0.08	0.06	10	27	22	27
Ka	VH	0.17	0.07	0.32	0.06	47	33	79	35
Ka	HV	0.17	0.06	0.32	0.06	46	34	80	35

polarization corresponds to radiation which was transmitted horizontally-polarized and which has depolarized, that is received with vertical polarization. We note that CryoSat-2 and AltiKa are altimeters that is nadir-looking, and KuKa was also deployed nadir-looking for this study. As shown in Figure 2 (and the SI Waveform Atlas), HH and VV waveforms are similar, as are VH and HV.

It is clear that the highest amplitude peaks and centroids in the co-pol data are at much smaller ranges and higher power than in the cross-polarized data (Table 1). For the HH waveforms, the mean depth of the highest amplitude peak was 1 and 2 cm below the air/snow interface in the Ku- and Ka-bands, respectively, indicating that the dominant scattering surface is very close to the upper surface of the new snow layer. The mean depth of the HH waveform centroids was 20% and 21% of the total snow depth in the Ku- and Ka-bands, respectively. In this study, the dominant scattering surface and waveform centroid is not the snow/ice interface. Cross-polarized waveform centroids are much deeper than the co-polarized in both frequency bands, and show frequency dependence. In our VH data, the mean depth of the waveform centroids was 91% and 79% of the total snow depth in the Ku- and Ka-bands, respectively.

We note that detection of the remnant snow/ice interface appears particularly challenging using either co- and cross-polarized waveforms and in either frequency. Whilst power is concentrated at or near the air/snow interface in the co-pol waveforms, most power is returned from within the remnant snow layer in the cross-polarized waveforms. We investigated KuKa-derived estimates of snow depth calculated using polarimetric techniques, by differencing HH and VH waveform peaks and centroids (Willatt et al., 2023). In Figure 3 the relationships between the measured- and KuKa-estimated snow depths are shown. For KuKa-derived versus total snow depths the strongest relationship is seen using Ku-band centroids, with an r^2 value of 0.76. Using Ku-band peaks the r^2 value is 0.33, and for both peaks and centroids the mean KuKa-estimated snow depths are around 70% of the mean measured total depth. Using the Ka-band waveforms results in r^2 values of 0.12 and 0.03 for centroids and peaks, respectively. Linear regressions against remnant snow layer depths showed similar r^2 values as for total snow depth: 0.26 and 0.76, with mean depths 82% and 86% of the measured remnant snow depths, using peaks and centroids, respectively. Regressing KuKa estimates against measured snow depths for the new snow layer, r^2 values were low at 0.15 and below (Figure S4 in Supporting Information S1). A larger data set would help to further examine the effect of new and remnant snow depths on the KuKa-derived snow depths, and we must emphasize that this is a small data set which suggests a promising technique but does not permit a full examination at this stage.

The polarimetric technique of differencing the Ku VH and HH centroid ranges (Figure 3f) therefore provided the best KuKa-retrieved snow depths. The mean KuKa-derived depth of 31 cm was closer to the mean measured remnant snow depth (38 cm) than the mean measured total snow depth (46 cm), but the equal r^2 values do not suggest that there is a stronger relationship between remnant than total and KuKa-derived snow depths. The two relationships have similar slopes of (0.48 vs. 0.46). The waveforms (Figure 2 and SI Waveform Atlas) show co-polarized peaks and centroids close to the air/snow interface and cross-polarized peaks and centroids close to, or within the remnant snow, that is not bounding the remnant snow layer.

10.1029/2024GL112870

4. Discussion

The co-polarized waveforms, where the radiation was transmitted and received with horizontal polarization (HH), as for CryoSat-2 SIRAL and SRAL AltiKa, showed that most of the scattering occurred close to the air/snow interface, not at the snow/ice interface, in line with surface-based studies (Willatt et al., 2010, 2023). For the cross-polarized waveforms, where the radiation was transmitted with horizontal polarization but received with vertical polarization (VH), peaks and centroids were much deeper, similar to Willatt et al. (2023), 91% and 79% of the total snow depth in the Ku- and Ka-bands, respectively. A change in polarization generating cross-polarized backscatter can occur due to multiple scattering (e.g., Du et al. (2010)) whilst co-polarized backscatter could occur from single scattering at the air/snow interface, as seen in this study. Morphological features for example depth hoar have previously have been shown to increase radar scattering in snow on Antarctic sea ice (Willatt et al., 2010). The large grains observed in the remnant snow (Figures 1c and 1d) likely contribute to the multiple scattering and change in polarization, though models of cross-polarized altimetry waveforms needed to further investigate this are not yet available. We also note that the study was conducted in April, so morphological features may occur in the new snow over time, increasing scattering in the new snow layer (e.g., as observed in austral spring by Willatt et al. (2010)).

Strong relationships between Ku-band polarimetric estimates and measured snow depths were seen using waveform centroids, with r^2 of 0.76 against both total, and remnant, measured snow depths. This also indicates that 24% of the variability is associated with other quantities which could include differences in snow density, grain characteristics (e.g., specific surface area or shape) or radar speckle. Unlike Willatt et al. (2023), KuKa-retrieved depths were smaller than measured depths, so an algorithm would need to be developed with this taken into account. Relatively weak relationships between Ka-band polarimetric estimates and measured snow depths were seen in all cases, suggesting the Ka-band radiation did not penetrate as well through the remnant snow, or was scattered away from the sensor, or a combination, and we therefore conclude that Ku-band radiation was more suitable for snow depth estimation. The relationship between the measured snow depths was also investigated: the r^2 of a linear regression of remnant versus total snow depth is 0.95 and the r^2 values of new versus total is far lower, 0.19, indicating that the total snow depth is mostly determined by the remnant snow depth (Figure 3b).

Our findings suggest potential novel avenues for improved retrieval of snow depth and sea ice thickness over complex snowpacks. It is important to note that waveforms collected with a surface-based instrument may not be the same as those from a satellite sensor due to, for example, different frequencies, bandwidths, altitudes and footprints (Willatt et al., 2023). However, they provide information on where scattering may occur, e.g. close to the air/snow interface for co-polarized radiation, which could help explain observations at satellite scale e.g. Giles et al. (2008). Our results should not be interpreted as a survey of the radar-backscattering characteristics of all sea ice in the Weddell Sea. As we sampled ice floes that were relatively thick, the findings are more representative of multi year ice. Further work is needed to understand if these results hold for younger ice types and indeed a mixture of these ages generally found in the Weddell Sea. This means that our results will not represent the "average" radar properties of the sea ice in the region that would be observed by a satellite. Specifically, it was not possible to verify whether the surrounding, thinner first year ice might feature the idiosyncratic remnant snow cover we observed.

It is relevant to ask whether the characteristics of the remnant snow layer described here are common, or a relatively rare occurrence. For instance, was there a particularly large amount of snow on the ice floes at the beginning of summer 2021/2 that led to this layer of snow surviving? Several authors (e.g., Introduction of Andreas and Ackley (1982), Arndt et al. (2021)), have remarked on the absence of visible surface melt ponds on Antarctic sea ice, indicating that snow cover surviving the summer may be a common occurrence. Though melt can occur and lead to the formation of superimposed ice, the amount of melt is much less than in the Arctic (Haas et al., 2001).

We now address the spatial applicability of our results. 2022 and 2023 featured consecutive, record-low Antarctic sea ice extents of 1.97 and 1.79 million square kilometers respectively Turner et al. (2022), Gilbert and Holmes (2024). The data in this paper come from sea ice floes that were probably extant during the 2022 minimum extent, and therefore can only—at maximum—represent 1.97 million square kilometers of the total ice area in the subsequent 2022/23 growth season. However it can represent significant ice areas in the Weddell and Ross sectors of Antarctica and multi year sea ice has distinct geophysical properties from first year sea ice. Second and multi-year sea ice play a key role from a biological and glaciological perspective, acting as a *refugium* for sea ice dependent species at the summer minimum (e.g., Younger et al. (2015)) and exerting a geophysical influence on the nearby ice shelves (e.g., Ochwat et al. (2024), Massom et al. (2018)). The ability to accurately retrieve the thickness of this ice with satellite platforms may therefore allow these processes to be better understood.

This study provided insights into radar scattering over multi year sea ice in the Weddell Sea. Antarctica is dominated in its cold season by first year ice which can be geophysically distinct due to phenomena such as flooding (not observed in this campaign). Future studies of first-year ice and over flooded snow would therefore be needed to establish how/whether the techniques can be applied. Mission requirements of the CRISTAL satellite (Kern et al., 2020), operating in the Ku- and Ka-bands and due for launch in 2028, include retrieval of Antarctic sea ice thickness and the depth of its snow cover. An understanding of radar scattering over all sea ice and snow conditions in the Southern Ocean will be necessary for consistently accurate retrievals. Coincident Ku- and Ka-band measurements (similar to those made in the Ku-band in Willatt et al. (2010)) with data on snow characteristics (including density and depth) as well as waveform modeling will be needed.

5. Conclusion

We investigated co- and cross-polarized Ku- and Ka-band radar waveforms using a surface-based radar deployed over snow covered sea ice in the Weddell Sea. Two distinct layers were often observed in the snowpack: a “new” layer of snow from the 2022 cold season, and a “remnant” snow layer beneath, which had survived the previous summer's melt. This remnant snow exhibited large, heavily sintered grains, much higher density, and occasionally superimposed ice at the base. Over these snow packs, assumptions about scattering developed for Arctic sea ice (Laxon et al., 2003) are unlikely to hold. Polarimetric techniques offer a novel way to estimate coincident snow depths and sea ice elevations for thickness estimation. Since no current satellite altimeters have this capability, a new mission would have to be developed for snow depths to be retrieved polarimetrically.

Data Availability Statement

KuKa raw data were processed to waveforms using KuKaPy software (Mead et al., 2023) followed by averaging and polarimetric analysis (Willatt & Mallett, 2024). Additional code to produce Figures S1 and S2 in Supporting Information S1: Mallett and Willatt (2024). Figures 1b and S1 in Supporting Information S1 use Antarctic sea ice type data from Melsheimer et al. (2023) and Figure S1 in Supporting Information S1 uses sea ice drift data (OSI SAF, 2021).

Acknowledgments

We thank Povl Abrahamsen and David Barnes for contributing to data collection in the field, and are grateful for the support of the Polarstern crew, scientists and helicopter pilots of the Alfred Wegener Institute under the leadership of Mario Hopperma for expedition PS129. We are also grateful to Christian Melsheimer for advice on the ice type product (Melsheimer et al., 2023). RW, JS and JW acknowledge support from the NERC DEFIANT Grant (NE/W004712/1). RW, JS and VN acknowledge support from and European Space Agency NEOMI Grant 4000139243/22/NL/SD; JS also acknowledges funding via the Canada 150 chairs programme. RM acknowledges support from the London NERC Doctoral Training Partnership Grant (NE/L002485/1), the International Space Science Institute (Team no. 501) and from the Canada 150 chairs programme via JS. The work of TN was supported in part by European Space Agency (ESA) under Grant ESA/AO/1-9132/17/NL/MP, Grant ESA/AO/1-10061/19/I-EF, and Grant PO 5001027396; and in part by Natural Environment Research Council (NERC) under Grant NE/X004643/1.

References

Ackley, S. F., Lewis, M. J., Fritsen, C. H., & Xie, H. (2008). Internal melting in Antarctic sea ice: Development of “gap layers”. *Geophysical Research Letters*, *35*(11). https://doi.org/10.1029/2008GL033644

Andreas, E. L., & Ackley, S. F. (1982). On the differences in ablation seasons of Arctic and Antarctic sea ice. *Journal of the Atmospheric Sciences*, *39*(2), 440–447. https://doi.org/10.1175/1520-0469(1982)039⟨0440:OTDIAS⟩2.0.CO;2

Arndt, S., Haas, C., Meyer, H., Peeken, I., & Krumpen, T. (2021). Recent observations of superimposed ice and snow ice on sea ice in the northwestern Weddell Sea. *The Cryosphere*, *15*(9), 4165–4178. https://doi.org/10.5194/tc-15-4165-2021

Arndt, S., Maaß, N., Rossmann, L., & Nicolaus, M. (2024). From snow accumulation to snow depth distributions by quantifying meteoric ice fractions in the Weddell Sea. *The Cryosphere*, *18*(4), 2001–2015. https://doi.org/10.5194/tc-18-2001-2024

Du, J., Shi, J., & Rott, H. (2010). Comparison between a multi-scattering and multi-layer snow scattering model and its parameterized snow backscattering model. *Remote Sensing of Environment*, *114*(5), 1089–1098. https://doi.org/10.1016/J.RSE.2009.12.020

Garnier, F., Bocquet, M., Fleury, S., Bouffard, J., Tsamados, M., Remy, F., et al. (2022). Latest altimetry-based Sea Ice freeboard and volume inter-annual variability in the Antarctic over 2003–2020. *Remote Sensing*, *14*(19), 4741. https://doi.org/10.3390/RS14194741

Gilbert, E., & Holmes, C. (2024). 2023's Antarctic sea ice extent is the lowest on record. *Weather*, *79*(2), 46–51. https://doi.org/10.1002/wea.4518

Giles, K. A., Laxon, S. W., & Worby, A. P. (2008). Antarctic sea ice elevation from satellite radar altimetry. *Geophysical Research Letters*, *35*(3), 3503. https://doi.org/10.1029/2007GL031572

Haas, C., Thomas, D. N., & Bareiss, J. (2001). Surface properties and processes of perennial Antarctic sea ice in summer. *Journal of Glaciology*, *47*(159), 613–625. https://doi.org/10.3189/172756501781831864

Kacimi, S., & Kwok, R. (2020). The Antarctic sea ice cover from ICESat-2 and CryoSat-2: Freeboard, snow depth, and ice thickness. *The Cryosphere*, *14*(12), 4453–4474. https://doi.org/10.5194/TC-14-4453-2020

Kern, M., Cullen, R., Berruti, B., Bouffard, J., Casal, T., Drinkwater, M. R., et al. (2020). The Copernicus polar ice and snow topography altimeter (CRISTAL) high-priority candidate mission. *The Cryosphere*, *14*(7), 2235–2251. https://doi.org/10.5194/tc-14-2235-2020

Lawrence, I. R., Ridout, A. L., Shepherd, A., & Tilling, R. (2024). A simulation of snow on Antarctic sea ice based on satellite data and climate reanalyses. *Journal of Geophysical Research: Oceans*, *129*(1). https://doi.org/10.1029/2022JC019002

Laxon, S., Peacock, N., & Smith, D. (2003). High interannual variability of sea ice thickness in the Arctic region. *Nature*, *425*(6961), 947–950. https://doi.org/10.1038/nature02050

Mallett, R., & Willatt, R. (2024). KuKa Weddell ice type, floe location, tracing and snowfall analysis (version 1.0.2) [Software]. *Zenodo*. https://doi.org/10.5281/zenodo.11235298

Massom, R. A., Scambos, T. A., Bennetts, L. G., Reid, P., Squire, V. A., & Stammerjohn, S. E. (2018). Antarctic ice shelf disintegration triggered by sea ice loss and ocean swell. *Nature*, *558*(7710), 383–389. https://doi.org/10.1038/s41586-018-0212-1

Mead, J., Nandan, V., Willatt, R., & Newman, T. (2023). KuKaPy [Software]. *Zenodo*. https://doi.org/10.5281/zenodo.7967057

Meier, W. N., & Scott Stewart, J. (2023). *NSIDC land, ocean, coast, ice, and sea ice region masks*. NSIDC Special Report 25. (Tech. Rep.). National Snow and Ice Data Center.

Melsheimer, C., Spreen, G., Ye, Y., & Shokr, M. (2023). First results of Antarctic sea ice type retrieval from active and passive microwave remote sensing data. *The Cryosphere*, *17*(1), 105–126. https://doi.org/10.5194/tc-17-105-2023

Nab, C., Mallett, R., Gregory, W., Landy, J., Lawrence, I., Willatt, R., et al. (2023). Synoptic variability in satellite altimeter-derived radar freeboard of Arctic Sea Ice. *Geophysical Research Letters*, *50*(2). https://doi.org/10.1029/2022GL100696

Ochwat, N. E., Scambos, T. A., Banwell, A. F., Anderson, R. S., Maclennan, M. L., Picard, G., et al. (2024). Triggers of the 2022 Larsen B multi-year landfast sea ice breakout and initial glacier response. *The Cryosphere*, *18*(4), 1709–1731. https://doi.org/10.5194/tc-18-1709-2024

OSI SAF. (2021). Global low resolution Sea Ice drift [Dataset]. *EUMETSAT*. https://doi.org/10.15770/EUM_SAF_OSI_NRT_2007

Purich, A., & Doddridge, E. W. (2023). Record low Antarctic sea ice coverage indicates a new sea ice state. *Communications Earth & Environment*, *4*(1), 1–9. https://doi.org/10.1038/s43247-023-00961-9

Ricker, R., Hendricks, S., Perovich, D. K., Helm, V., & Gerdes, R. (2015). Impact of snow accumulation on CryoSat-2 range retrievals over Arctic sea ice: An observational approach with buoy data. *Geophysical Research Letters*, *42*(11), 4447–4455. https://doi.org/10.1002/2015GL064081

Stroeve, J., Nandan, V., Willatt, R., Tonboe, R., Hendricks, S., Ricker, R., et al. (2020). Surface-based Ku- and Ka-band polarimetric radar for sea ice studies. *The Cryosphere*, *14*(12), 4405–4426. https://doi.org/10.5194/tc-14-4405-2020

Turner, J., Holmes, C., Caton Harrison, T., Phillips, T., Jena, B., Reeves-Francois, T., et al. (2022). Record low Antarctic sea ice cover in February 2022. *Geophysical Research Letters*, *49*(12), e2022GL098904. https://doi.org/10.1029/2022GL098904

Ulaby, F., Long, D., Blackwell, W., Elachi, C., Fung, A., Ruf, C., et al. (2014). *Microwave radar and radiometric remote sensing*. The University of Michigan Press.

Vincent, P., Steunou, N., Caubet, E., Phalippou, L., Rey, L., Thouvenot, E., & Verron, J. (2006). AltiKa: A Ka-band altimetry payload and system for operational altimetry during the GMES period. *Sensors*, *6*(3), 208–234. https://doi.org/10.3390/S6030208

Willatt, R., Giles, K. A., Laxon, S. W., Stone-Drake, L., & Worby, A. P. (2010). Field investigations of Ku-band radar penetration into snow cover on Antarctic sea ice. *IEEE Transactions on Geoscience and Remote Sensing*, *48*(1), 365–372. https://doi.org/10.1109/TGRS.2009.2028237

Willatt, R., Laxon, S., Giles, K., Cullen, R., Haas, C., & Helm, V. (2011). Ku-band radar penetration into snow cover on Arctic sea ice using airborne data. *Annals of Glaciology*, *52*(57), 197–205. https://doi.org/10.3189/172756411795931589

Willatt, R., & Mallett, R. (2024). KuKa Weddell waveform processing (version 1.0.0) [Software and Dataset]. *Zenodo*. https://doi.org/10.5281/zenodo.11472778

Willatt, R., Stroeve, J. C., Nandan, V., Newman, T., Mallett, R., Hendricks, S., et al. (2023). Retrieval of snow depth on Arctic Sea Ice from surface-based, polarimetric, dual-frequency radar altimetry. *Geophysical Research Letters*, *50*(20), e2023GL104461. https://doi.org/10.1029/2023GL104461

Wingham, D. J., Francis, C. R., Baker, S., Bouzinac, C., Brockley, D., Cullen, R., et al. (2006). CryoSat: A mission to determine the fluctuations in Earth's land and marine ice fields. *Advances in Space Research*, *37*(4), 841–871. https://doi.org/10.1016/j.asr.2005.07.027

Worby, A. P., Geiger, C. A., Paget, M. J., Van Woert, M. L., Ackley, S. F., & DeLiberty, T. L. (2008). Thickness distribution of Antarctic sea ice. *Journal of Geophysical Research*, *113*(5). https://doi.org/10.1029/2007JC004254

Younger, J. L., Clucas, G. V., Kooyman, G., Wienecke, B., Rogers, A. D., Trathan, P. N., et al. (2015). Too much of a good thing: Sea ice extent may have forced emperor penguins into Refugia during the last glacial maximum. *Global Change Biology*, *21*(6), 2215–2226. https://doi.org/10.1111/gcb.12882

References From the Supporting Information

Melsheimer, C., & Spreen, G. (2022). Sea ice type data for the Antarctic [Dataset]. *UNI-BREMEN*. https://seaice.uni-bremen.de/data/MultiYearIce/ascat-amsr2/raw/